

Correlation between structure and intervalence charge-transfer transitions in nanocrystalline $\text{CoFe}_{2-x}\text{M}_x\text{O}_4$ ($M=\text{Mn,Al,Sc}$) thin films

Biao Zhou, Ya-Wen Zhang, Yue-Jun Yu, Chun-Sheng Liao, and Chun-Hua Yan*

State Key Laboratory of Rare Earth Materials Chemistry and Applications and Joint Laboratory of Peking University and The University of Hong Kong on Rare Earth Materials and Bioinorganic Chemistry, College of Chemistry and Molecular Engineering, Peking University, Beijing 100871, China

Liang-Yao Chen and Song-You Wang

Department of Optical Science and Engineering, Fudan University, Shanghai 200433, China

(Received 25 October 2002; revised manuscript received 19 February 2003; published 30 July 2003)

The structures, magnetisms, and magneto-optical (MO) Kerr spectra of nanocrystalline $\text{CoFe}_{2-x}\text{M}_x\text{O}_4$ ($M = \text{Mn, Al, Sc}$) thin films have been systematically investigated by means of x-ray diffraction, atomic force microscopy, alternating gradient magnetometer, and MO Kerr spectrometer. The results revealed that the intervalence charge transfer (IVCT) transition of $[\text{Co}^{2+}]t_{2g} \rightarrow \text{O}^{2-} \rightarrow [\text{Fe}^{3+}]t_{2g}$ in those nanocrystalline films had a strong correlation to the structures created by doping with those trivalent metal ions, within the miscibility range of spinel structure. Doping with Al^{3+} and Sc^{3+} ions led to the increase and decrease of the energy of the IVCT transition, respectively. On the other hand, doping with Mn^{3+} has weak effect on the energy. The molecular orbital theory of IVCT transitions was employed to account for the dependence of the transition energy on the structures. It is concluded that the position of the Kerr rotation peak of the IVCT transition can be adjusted by doping with different trivalent cations and controlling the doping content due to doping induced structural changes.

DOI: 10.1103/PhysRevB.68.024426

PACS number(s): 34.70.+e, 78.20.Ls, 75.75.+a, 75.50.Gg

I. INTRODUCTION

Spinel ferrites have a general formula of $\text{Me}^{2+}\text{Fe}_2^3+\text{O}_4$ ($\text{Me}^{2+} = \text{Fe}^{2+}, \text{Co}^{2+}, \text{Ni}^{2+}, \text{etc.}$). In the cubic spinel type structure,^{1,2} O^{2-} ions form the close-packed face-centered-cubic (fcc) lattice. In this lattice, only two types of cation sites named tetrahedral (*A* site) and octahedral (*B* sites) exist, and the cation distribution formula is commonly expressed as $(A)[B]_2\text{O}_4$, where the parentheses and square brackets denote *A* sites and *B* sites, respectively. Due to the existence of confused interpretations of the relationship between the electronic structure and magneto-optical (MO) properties, *d-d* charge-transfer transitions, and MO spectra of spinel ferrites have been attracting considerable interest in the past 20 years.^{3,4} The MO properties of a number of spinel ferrites were investigated by Fontijn and co-workers.⁵⁻⁸ Two types of interactions, i.e., the crystal field (CF) transition and charge-transfer transitions including the intervalence charge-transfer (IVCT) transition and intersublattice charge-transfer (ISCT) transition, have been identified in the MO spectra.⁵⁻¹¹ It was proved that the IVCT transition is one of the major interactions governing the MO properties.

The IVCT transition is a process in which an electron from a cation is transferred to a neighboring cation through optical excitation.¹² Typically in Fe_3O_4 ,¹³⁻¹⁵ the $3d-3d$ IVCT transition takes places between Fe^{2+} and Fe^{3+} ions both in *B* sites, and can be mediated by O^{2-} ions; thus it is expressed as $[\text{Fe}^{2+}]-\text{O}^{2-}-[\text{Fe}^{3+}] \leftrightarrow [\text{Fe}^{3+}]-\text{O}^{2-}-[\text{Fe}^{2+}]$. In such an IVCT transition, Fontijn and co-workers suggested that the electrostatic polarization of O^{2-} ions plays a significant role in determining the energy of this transition.⁵⁻⁷

Cobalt ferrite CoFe_2O_4 has drawn much attention for its

strong MO effect in the visible range.^{16,17} The polar MO Kerr spectra of CoFe_2O_4 film deposited by spray pyrolysis on fused silicon substrates had been reported by Martens and co-workers.¹⁸⁻²¹ There were two Kerr rotation peaks at 2.0 and 2.2 eV for Co ferrite thin films in the visible range (1.55–3.1 eV). The rotation peak at 2.2 eV was assigned to an IVCT transition from $[\text{Co}^{2+}]$ to $[\text{Fe}^{3+}]$ at *B* sites, illustrated as $[\text{Co}^{2+}]t_{2g} \rightarrow \text{O}^{2-} \rightarrow [\text{Fe}^{3+}]t_{2g}$. The rotation peak at 2.0 eV was ascribed to the CF transition of (Co^{2+}) at *A* sites, expressed as ${}^4A_2({}^4F) \rightarrow {}^4T_1({}^4P)$.²² However, the relationship between the structures and IVCT transitions in Co ferrite thin film is still a subject of debate.

More recently, we used Mn^{3+} ions ($r_{\text{VI}}=0.0645$ nm with high spin state²³) as the dopant to substitute Fe^{3+} ions ($r_{\text{VI}}=0.0645$ nm with high spin state²³) in nanocrystalline CoFe_2O_4 thin films.^{24,25} It was demonstrated that doping of Mn^{3+} ions could effectively lower the T_C of Co ferrite, and considerable improvement of the MO effect has been achieved through a cubic-to-tetragonal phase transition and the generation of a new Kerr rotation at 1.9 eV. To further understand the doping effect on MO properties and the new active MO Kerr rotation in $\text{CoFe}_{2-x}\text{Mn}_x\text{O}_4$ films, trivalent metal ions with altered radius such as Al^{3+} [$r_{\text{VI}}=0.0535$ nm (Ref. 23)] and Sc^{3+} [$r_{\text{VI}}=0.0745$ nm (Ref. 23)] ions, which have no unpaired or *d* electrons in their electronic configurations, were doped into CoFe_2O_4 films. The objective of this study is to systematically investigate the correlation between the structures and IVCT transitions in nanocrystalline $\text{CoFe}_{2-x}\text{M}_x\text{O}_4$ ($M = \text{Mn, Al, Sc}$) thin films. We found that the energy of IVCT transitions was highly correlative with the structures of those spinel ferrites. For further understanding the doping effects on the structures,

four typical compositions of powder samples were prepared, and the structural information was extracted by Rietveld refinement. Based on these studies, molecular orbital theory was used to explain the correlation between the structures and IVCT transition in the as-deposited films. From the experimental results we conclude that the position of the Kerr rotation peak can be adjusted by doping various trivalent cations and controlling the doping content x due to doping induced structural changes.

II. EXPERIMENT

Nanocrystalline $\text{CoFe}_{2-x}\text{Mn}_x\text{O}_4$ ($x=0-1.0$), $\text{CoFe}_{2-x}\text{Al}_x\text{O}_4$ ($x=0-1.0$), and $\text{CoFe}_{2-x}\text{Sc}_x\text{O}_4$ ($x=0-0.4$) thin films were prepared by a modified Pechini-type sol-gel method.²⁶⁻²⁸ Appropriate portions of $\text{Fe}(\text{NO}_3)_3$ [analytical reagent (AR)], $\text{Co}(\text{NO}_3)_2$ (AR), and $\text{Mn}(\text{NO}_3)_2$ [$\text{Al}(\text{NO}_3)_3$ or $\text{Sc}(\text{NO}_3)_3$] (AR) were dissolved in a water-alcohol solution (1/8 in v/v). Then, quantitative amount of citric acid (AR) and poly-(ethylene glycol) (PEG, molecular weight $\sim 20\,000$, chemically pure) were also dissolved in the above solution. Upon stirring for 2 h, a homogeneous polymeric precursor solution was obtained. This precursor solution was spin-coated onto the monocrystalline silicon (100) substrate at a speed of about 4000 rpm for 8 s. The solvents and organics in the coatings can be removed by drying in an electric oven at 100–110 °C and subsequently preannealed in a tubular furnace at 400 °C under an oxygen-flowing atmosphere. The resulted precursor films after 10 coating cycles were finally annealed at 700 °C for 1 h, and the $\text{CoFe}_{2-x}\text{M}_x\text{O}_4$ films were thus obtained. The film thickness is determined by scanning electron microscopy (SEM, Amarty-1910, USA).

For the preparation of amorphous powders, the above precursor solutions were dried in an electric oven and then preannealed in the tubular furnace at 400 °C under an oxygen atmosphere. Finally, the as-derived powders were annealed in a muffle furnace at 1200 °C for 12 h in still air. An inductively coupled plasma (ICP) atomic emission spectroscopy (AES) analysis reported the same stoichiometry for the elements of Co, Fe, Mn, Al, and Sc in all the powder samples as expected.

The crystal structures of the films were characterized by x-ray diffraction (XRD) ($D_{\text{max}}-2000$, Rigaku, Japan) from 15° to 65° with a 2θ speed of 4°/min, and the XRD data of powder samples for Rietveld refinement were collected from 15° to 135° with a 2θ speed of 1°/min by another diffractometer ($D_{\text{max}}-2500$, Rigaku, Japan), using $\text{Cu } K\alpha$ radiation ($\lambda = 1.5418 \text{ \AA}$). The surface morphologies of the nanocrystalline films were observed by atomic force microscopy (AFM, AutoProbe CP, PSI, USA) with a 5 μm scanner. The magnetic measurement of the samples was performed on an alternating gradient magnetometer (AGM, MicroMag™ 2900, USA) at room temperature. The hysteresis loops were recorded in fields up to 15 kOe for all samples. The external fields were applied parallel to the film plane in the magnetic measurements. The magnetization values presented in this paper are in conventional cgs electromagnetic units (emu),

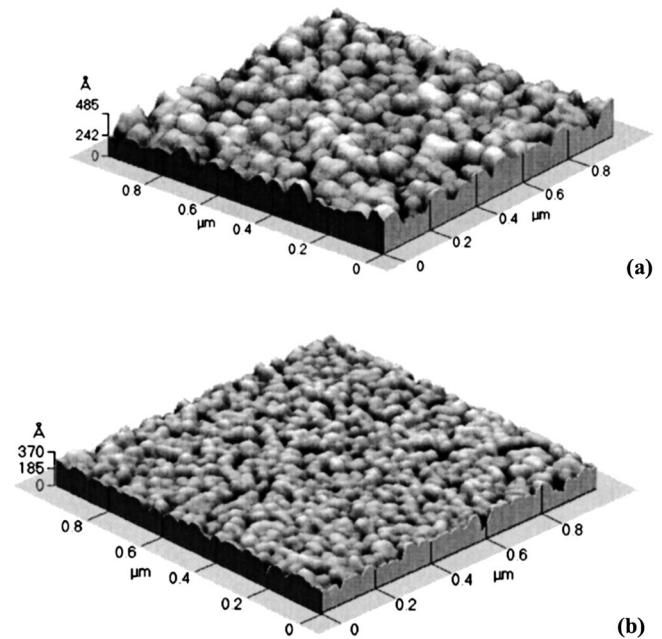


FIG. 1. 3D AFM micrographs of nanocrystalline (a) CoFeMnO_4 and (b) $\text{CoFe}_{1.6}\text{Al}_{0.4}\text{O}_4$ thin films annealed at 700 °C for 1 h.

and the antimagnetic contribution from silicon substrates was taken out.

The polar Kerr spectra were recorded by the MO Kerr spectrometer setup by us, under an applied field of 10 kOe perpendicular to the film plane at room temperature. A 150 W Xe short-arc lamp was used as a continuum light source to cover the 1.55–3.1 eV visible spectral range. The Kerr rotation θ_K was taken as $\theta_K = \frac{1}{2} [\theta_K(M) - \theta_K(-M)]$, where M is the magnetization, in order to eliminate the contribution on MO rotation from nonmagnetic substrates.

III. RESULTS

A. Structures

With the modified Pechini-type sol-gel method, nanocrystalline $\text{CoFe}_{2-x}\text{M}_x\text{O}_4$ ($M = \text{Mn, Al, Sc}$) thin films were easily prepared after annealing at 700 °C for 1 h. Figure 1 typically shows the three-dimensional (3D) images of CoFeMnO_4 and $\text{CoFe}_{1.6}\text{Al}_{0.4}\text{O}_4$ films as probed by AFM. These films are distinctly composed of ultrafine grains in the average grain size of 50 and 25 nm (in diameter), respectively. Due to that the root mean square roughness of the sol-gel-derived films measured by AFM is only 3–5 nm, the nanograins showed a narrow size distribution.

Figure 2 representatively exhibits the XRD patterns of CoFe_2O_4 , $\text{CoFe}_{1.6}\text{Mn}_{0.4}\text{O}_4$, $\text{CoFe}_{1.6}\text{Al}_{0.4}\text{O}_4$, and $\text{CoFe}_{1.8}\text{Sc}_{0.2}\text{O}_4$ films. All reflections of the film samples correspond to a spinel structure, and no extra peaks attributed to other phases were observed, indicating that Mn^{3+} , Al^{3+} , or Sc^{3+} ions can be thoroughly doped into the spinel lattice in the present work. According to the Bragg equation, lattice constant a values of the samples were calculated by a least-squares method.^{29,30} Figure 3 depicts the calculated lattice constants of the $\text{CoFe}_{2-x}\text{M}_x\text{O}_4$ ($M = \text{Mn, Al, Sc}$) films as a

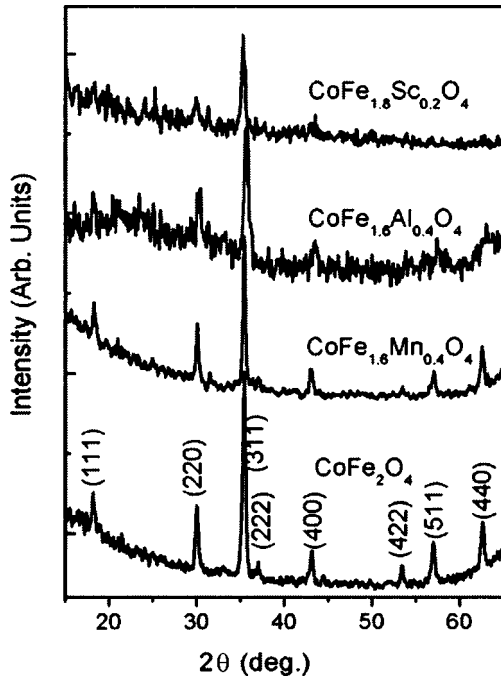


FIG. 2. XRD patterns of the as-deposited CoFe_2O_4 , $\text{CoFe}_{1.6}\text{Mn}_{0.4}\text{O}_4$, and $\text{CoFe}_{1.6}\text{Al}_{0.4}\text{O}_4$ films annealed at 700°C for 1 h.

function of the doping content x . Due to the fact that the ion radius of Mn^{3+} is compatible to that of Fe^{3+} , the substitution of Fe^{3+} with Mn^{3+} ion led to no obvious changes in a . However, a notable increase and decrease in a were observed for the substitution of Fe^{3+} with Sc^{3+} and Al^{3+} ions, respectively. From Fig. 3, it can be also found that a changed monotonically with x for Sc^{3+} - or Al^{3+} -doped films.

The mean grain size D (in diameter) was calculated by the Sherrer equation,³¹ $D = K\lambda / (\beta \cos \theta)$, where K is a dimensionless constant ($K = 0.9$, usually), 2θ is the diffraction

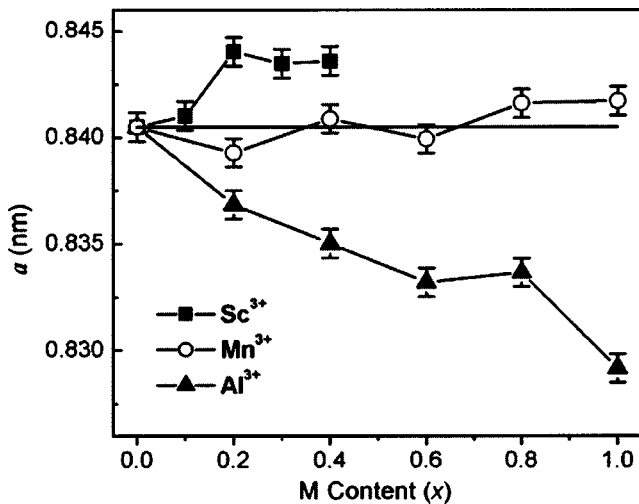


FIG. 3. Plot of the lattice constant a as a function of the doping content x with the error bar for $\text{CoFe}_{2-x}\text{M}_x\text{O}_4$ ($M = \text{Mn}, \text{Al}, \text{Sc}$) films annealed at 700°C for 1 h. The straight line indicates a of pure CoFe_2O_4 film.

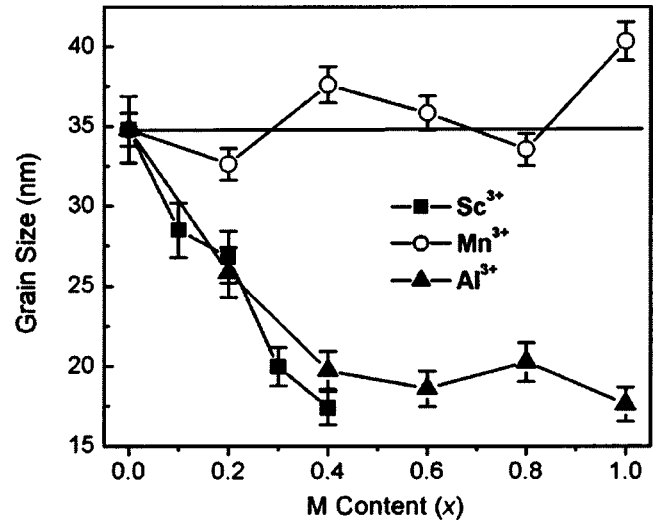


FIG. 4. Plot of the mean grain size as a function of the doping content x with the error bar for $\text{CoFe}_{2-x}\text{M}_x\text{O}_4$ ($M = \text{Mn}, \text{Al}, \text{Sc}$) films annealed at 700°C for 1 h. The straight line indicates mean grain size of pure CoFe_2O_4 film.

angle, λ is the wavelength of the x-ray radiation, and β is the full width at half maximum of the diffraction peak calibrated from high purity silicon (in radians). Figure 4 shows the plot of the mean grain size of the as-deposited films as a function of the doping content x . The grain size was observed to decrease with x when doping with Al^{3+} or Sc^{3+} ions, which was also confirmed by the AFM analysis. Perhaps it is because of the structural mismatch, arising from the large discrepancy in the ion radii of Al^{3+} and Sc^{3+} compared with that of Fe^{3+} , that doping of Al^{3+} or Sc^{3+} ions could suppress the nuclei formation during the film growth. However, the grain size was almost kept unchanged in the Mn^{3+} -doped films, owing to the finding that the substitution of Fe^{3+} with Mn^{3+} ions could not induce any structural mismatch for their compatible ion radii.

B. Magnetic behaviors

In a normal-type spinel ferrite, the divalent cations locate at A sites. However, CoFe_2O_4 is regarded as an inverse-type spinel with a cubic structure and has a cation distribution of $(\text{Fe}^{3+})_A[\text{Co}^{2+}\text{Fe}^{3+}]_B\text{O}_4$.³² Nevertheless, small CoFe_2O_4 particles may have a nonequilibrium cation distribution with some A sites occupied by Co^{2+} ions.^{33,34} In most cases, the properties of spinel ferrites are highly correlative with such a cation distribution, especially for the magnetism.

In general, spinel structure ferrites behave as ferrimagnets, as a result of the magnetizations of them [$M(x)$], which are the net moments of A and B sites (M_A and M_B), and given by $M(x) = M_B(x) - M_A(x)$. Due to the fact that the metal ions of Co^{2+} , Mn^{3+} , Al^{3+} , and Sc^{3+} ions have a stronger capability to occupy the B sites than Fe^{3+} ions,^{35,36} the structural formula of $\text{CoFe}_{2-x}\text{M}_x\text{O}_4$ ($M = \text{Mn}, \text{Al}, \text{Sc}$) may be written as $(\text{Fe})[\text{CoFe}_{1-x}\text{M}_x]\text{O}_4$ ($0 < x < 1$). Figure 5 gives the measured values of the saturation magnetization (M_S) as a function of x for $\text{CoFe}_{2-x}\text{M}_x\text{O}_4$ (M

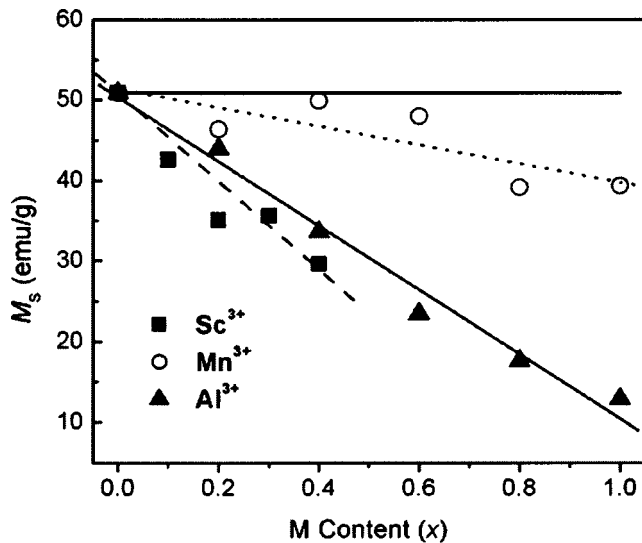


FIG. 5. Measured and calculated values of magnetization (M_S) as a function of doping content x for $\text{CoFe}_{2-x}\text{M}_x\text{O}_4$ ($M = \text{Mn, Al, Sc}$) films annealed at 700°C for 1 h.

$=\text{Mn, Al, Sc}$) thin films. It can be found that all M_S of the doped sample decreases linearly with increasing x . Because the experimental moment of Mn^{3+} ($4.9\mu_B$) is slightly smaller than that of Fe^{3+} ($5.9\mu_B$), only a slight decrease in M_S with increasing doping content x was observed. However, the notable decrease in M_S is observed for both $\text{CoFe}_{2-x}\text{Al}_x\text{O}_4$ and $\text{CoFe}_{2-x}\text{Sc}_x\text{O}_4$ films because Al^{3+} and Sc^{3+} are nonmagnetic ions.

The large coercive force (H_C) of Co ferrite predominantly arises from the single-ion anisotropy of Co^{2+} ions on the B sites.³² Figure 6 displays the variation of H_C with x for $\text{CoFe}_{2-x}\text{M}_x\text{O}_4$ ($M = \text{Mn, Al, Sc}$) thin films. It is noted that H_C of all the doped samples decreases with increasing x . It is considered that the content decrease of Co^{2+} ions at the B sites resulted in the decrease of H_C . However, H_C of

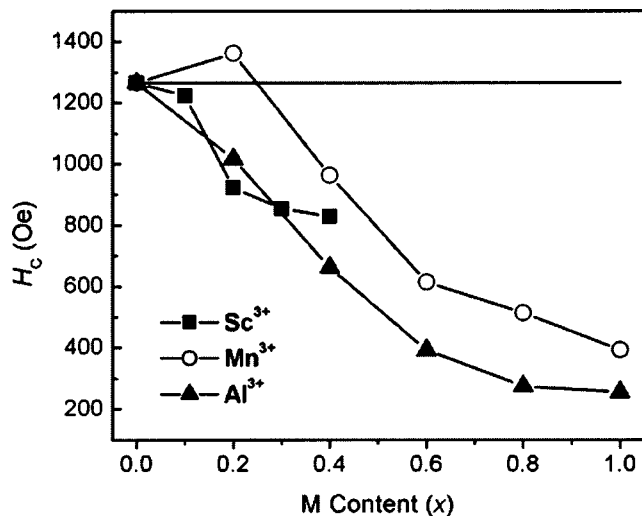


FIG. 6. Variation of the coercive force (H_C) with the doping content x for $\text{CoFe}_{2-x}\text{M}_x\text{O}_4$ ($M = \text{Mn, Al, Sc}$) films annealed at 700°C for 1 h.

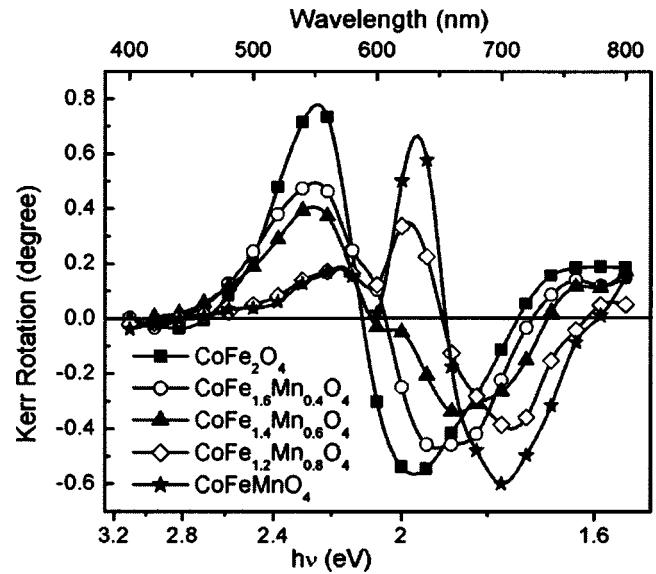


FIG. 7. Wavelength dependence of polar Kerr rotations for $\text{CoFe}_{2-x}\text{Mn}_x\text{O}_4$ ($x = 0 - 1.0$) films annealed at 700°C for 1 h.

$\text{CoFe}_{2-x}\text{Al}_x\text{O}_4$ and $\text{CoFe}_{2-x}\text{Sc}_x\text{O}_4$ decreases more quickly than that of $\text{CoFe}_{2-x}\text{Mn}_x\text{O}_4$, which is possibly correlated with the migration of more Co^{2+} ions from B to A sites by doping with Al^{3+} and Sc^{3+} ions than that by doping with Mn^{3+} ions. Furthermore, the reduced grain size also brought about the decrease of H_C , which in turn could cause H_C of $\text{CoFe}_{2-x}\text{Mn}_x\text{O}_4$ to be larger than that of $\text{CoFe}_{2-x}\text{Al}_x\text{O}_4$ and $\text{CoFe}_{2-x}\text{Sc}_x\text{O}_4$ for a given doping content.

C. Magneto-optical properties

Since a slight difference in the thickness of spinel ferrites deposited on Si substrate would induce drastic changes in the Kerr spectra,³⁷ in the present work, all the films for MO measurements were controlled to have the same thickness of 200 ± 3 nm (determined by SEM) for convenience in comparing the experimental results. Hereafter, we will focus on the Kerr spectra of the as-deposited films, based on the assumption that they have similar optical components.

The polar Kerr spectra of $\text{CoFe}_{2-x}\text{M}_x\text{O}_4$ films are presented in Figs. 7–9. These spectra were similarly observed by Martens *et al.* for the CoFe_2O_4 film deposited on monocrystalline silicon,^{18,19} but were quite different from the polar Kerr spectrum of the single crystal of CoFe_2O_4 and Faraday spectra of CoFe_2O_4 films on transparent substrates.³⁷ From Figs. 7–9, we can find that there are two Kerr rotation peaks at 2.0 and 2.25 eV for the pure Co ferrite. Perhaps due to the systemic error coming out from the different MO Kerr spectrometer, our results showed a slight difference in the energy of the transitions from that obtained by Kim *et al.* (2.0 and 2.2 eV).²²

From Figure 7, it is noted that doping of Mn^{3+} led to the decline, even the disappearance of the Kerr rotation at 2.25 eV ascribed to the IVCT transition, while a new peak at 1.9 eV appeared. The Kerr rotation peak at 1.9 eV increased with the doping content x , whereas that at 2.25 eV decreased with increasing x . Normally, Mn^{3+} ion preferably occupies B

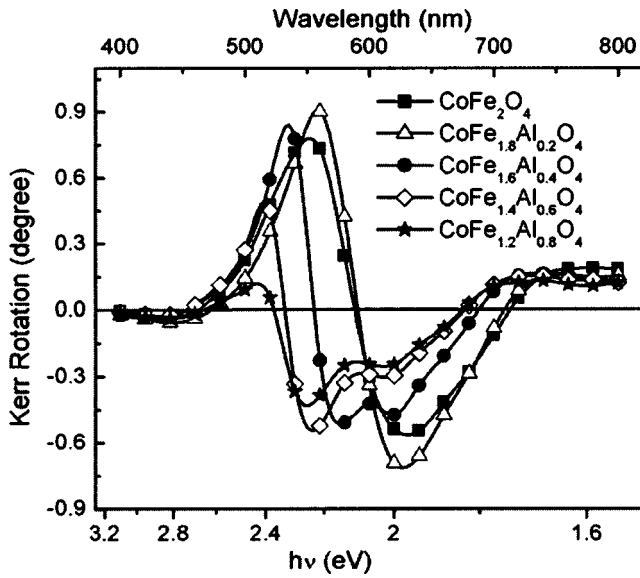


FIG. 8. Wavelength dependence of polar Kerr rotations for $\text{CoFe}_{2-x}\text{Al}_x\text{O}_4$ ($x=0-0.8$) films annealed at 700°C for 1 h.

sites in replacement of most Fe^{3+} ions and makes a few Co^{2+} ions migrate from B to A sites. The decrease of the peak at 2.25 eV distinctly is a result of the decrease in occupancy rate of both Co^{2+} and Fe^{3+} ions at B sites. When x is higher than 1.0 , this peak disappeared because Fe^{3+} ions at B sites were wholly substituted by Mn^{3+} ions.

From Figure 8, we can see that, for $\text{CoFe}_{2-x}\text{Al}_x\text{O}_4$ films, the rotation peak at 2.25 eV assigned to the IVCT transition decreased with increasing Al content, and the peak was slowly blueshifted with the increase in x . Generally, Al^{3+} ions predominately occupy B sites.³⁶ However, Al^{3+} ions can partially occupy A sites in the case of nanocrystalline films; thus the content decrease of both Co^{2+} and Fe^{3+} ions at B sites would reduce the Kerr rotation associated with the

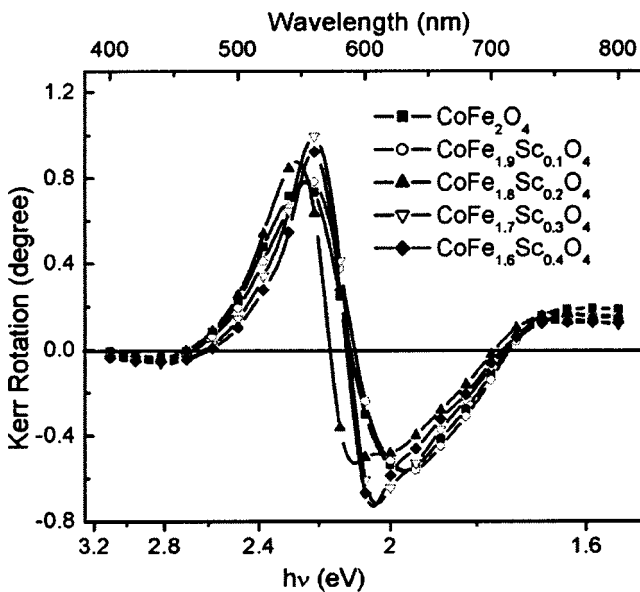


FIG. 9. Wavelength dependence of polar Kerr rotations for $\text{CoFe}_{2-x}\text{Sc}_x\text{O}_4$ ($x=0-0.4$) films annealed at 700°C for 1 h.

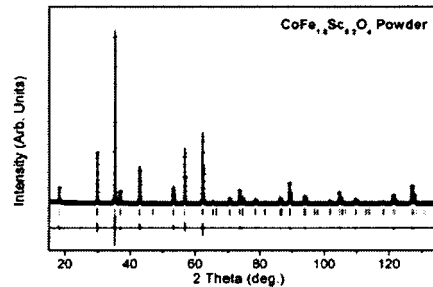
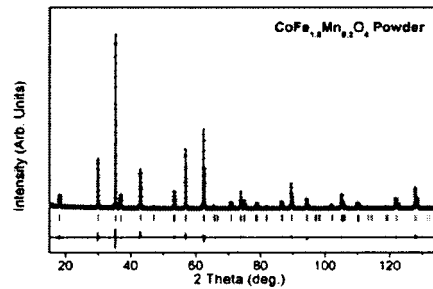
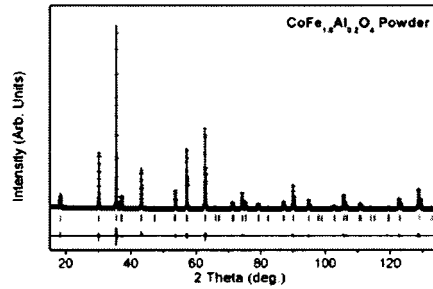
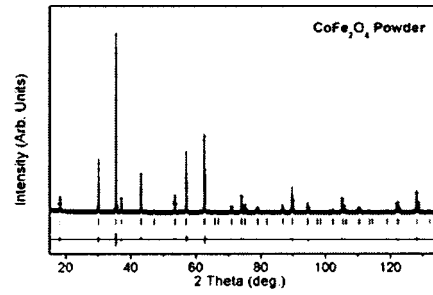


FIG. 10. Experimental (solid lines) and calculated by Rietveld refinement (crosses) XRD patterns for pure CoFe_2O_4 and $\text{CoFe}_{1.8}M_{0.2}\text{O}_4$ ($M=\text{Mn},\text{Al},\text{Sc}$) powder annealed at 1200°C for 12 h. Differences between the experimental and calculated intensity are shown in the bottom, and the small bars indicate the angular positions of the allowed Bragg reflection.

IVCT transition. When x is higher than 0.8 , the Kerr rotation peak almost disappeared with Al^{3+} substitution.

Opposite to the Al-doped films, the presence of Sc^{3+} ions caused the increase of the rotation peak at 2.25 eV assigned to the IVCT transition with x in Fig. 9. In addition, this peak was slowly redshifted with the increase in x . Sc^{3+} ions could only occupy B sites because of their large ion radius and hence caused the decreased content of both Co^{2+} and Fe^{3+} ions at B sites. In contrast, the Kerr rotation increased with

TABLE I. Structural parameters, pattern R factor (R_p), weighted pattern R factor (R_{WP}), A -O (d_{A-O}) and B -O (d_{B-O}) bond lengths, B - B distance (d_{B-B}), and B -O- B bond angle (θ) of CoFe_2O_4 and $\text{CoFe}_{1.8}M_{0.2}\text{O}_4$ ($M = \text{Mn, Al, Sc}$) powder samples, which were deduced from the Rietveld refinement of XRD data.

Sample	CoFe_2O_4	$\text{CoFe}_{1.8}\text{Al}_{0.2}\text{O}_4$	$\text{CoFe}_{1.8}\text{Mn}_{0.2}\text{O}_4$	$\text{CoFe}_{1.8}\text{Sc}_{0.2}\text{O}_4$
a (nm)	0.83989(2)	0.83720(2)	0.84014(2)	0.84295(3)
d_{A-O} (nm)	0.1916(1)	0.1920(1)	0.1913(1)	0.1905(1)
d_{B-O} (nm)	0.2045(1)	0.2033(1)	0.2047(1)	0.2062(1)
$R(d_{A-O}/d_{B-O})$	0.937	0.944	0.935	0.924
d_{B-B} (nm)	0.2969(1)	0.2960(1)	0.2970(1)	0.2980(1)
θ_{B-O-B} (deg)	93.10(2)	93.43(2)	93.00(2)	92.53(2)
R_p (%)	7.44	7.41	7.89	9.47
R_{WP} (%)	10.71	10.50	10.96	13.42

x , indicating that doping with Sc^{3+} would enhance the Kerr rotation of CoFe_2O_4 .

Since the ion radius of Mn^{3+} is compatible to that of Fe^{3+} , the Kerr rotation peak at 2.25 eV associated with the IVCT transition displayed only slight shifting. The new Kerr rotation peak at 1.9 eV in these films was indeed induced by the doping of Mn^{3+} ions for it increases with Mn^{3+} content x , but did not originate from the substitution effects on the structures. Due to the fact that CF transitions at B sites are spin-forbidden, the new Kerr rotation is likely ascribable to the IVCT transition from $[\text{Co}^{2+}]$ to $[\text{Mn}^{3+}]$ at the B sites. Because the electron acceptability of Mn^{3+} is stronger than that of Fe^{3+} , the energy of the IVCT transition from $[\text{Co}^{2+}]$ to $[\text{Mn}^{3+}]$ is lower than that to $[\text{Fe}^{3+}]$. Therefore, the new Kerr rotation peak exhibited a redshift and increased with x .

IV. DISCUSSION

In order to estimate the doping effect on the structures in detail, we used the Rietveld refinement to extract the structural information from the XRD patterns of four typical powder samples of CoFe_2O_4 and $\text{CoFe}_{1.8}M_{0.2}\text{O}_4$ ($M = \text{Mn, Al, Sc}$) by the software of General Structure Analysis System (GSAS).³⁸ The calculated results were displayed in Figure 10. And the detailed structure information, such as the lattice constant, bond length and bond angle, is summarized in Table I. a values of $\text{CoFe}_{1.8}M_{0.2}\text{O}_4$ are 0.83989, 0.83720, 0.84014, and 0.84295 nm for $M = \text{Fe, Al, Mn, and Sc}$, respectively. If compared with the data shown in Fig. 3, the lattice constants of the powder samples are distinctly well consistent with the trend of that of the film samples against the variety of M^{3+} ions.

In general, spinel ferrite structure has 8 formula units (56 atoms) in a primitive cell. The space group is $O_h^7 Fd-3m$ (no. 227). In a standard spinel type lattice without any distortion, the fractional coordinates of A site, B site, and O^{2-} ion are $(1/8, 1/8, 1/8)$, $(1/2, 1/2, 1/2)$, and $(1/4, 1/4, 1/4)$, respectively. Therefore, the ratio (R) of the distance of A -O ($d_{A-O} = a\sqrt{3}/8$) to that of B -O ($d_{B-O} = a/4$) is 0.866. From Table I, it was observed that d_{B-O} also follows the trend of a against the dopant variety. The d_{B-O} values of $\text{CoFe}_{1.8}M_{0.2}\text{O}_4$ are 0.2045, 0.2033, 0.2047, and 0.2062 nm for $M = \text{Fe, Al,$

Mn, and Sc , respectively. However, d_{A-O} displayed a contrary trend to that of a and d_{B-O} . The d_{A-O} values of $\text{CoFe}_{1.8}M_{0.2}\text{O}_4$ are 0.1916, 0.1920, 0.1913 and 0.1905 nm for $M = \text{Fe, Al, Mn, and Sc}$, respectively. In addition, R values of all samples are larger than 0.866, and R will gradually decrease to 0.866 with increasing a . Correspondingly, the bond angles of B -O- B of all samples are larger than 90° , and also decrease to 90° when doping with Sc^{3+} ions. As we know, every B site is coordinated by six O^{2-} ions, and every O^{2-} ion is coordinated only by three B sites. Therefore, all the bond angles of B -O- B are larger than 90° owing to the spatial repulsion originating from the unsymmetrical coordination environment of O^{2-} ions, which result in the lattice distortion.

Furthermore, to elucidate the correlation between structures and d - d IVCT transitions in the nanocrystalline $\text{CoFe}_{2-x}M_x\text{O}_4$ ($M = \text{Mn, Al, Sc}$) thin films, the doping effects on the MO spectra were examined. Also from Figs. 8 and 9, we can clearly observe that doping with various trivalent metal ions exerted a strong influence on the position of Kerr

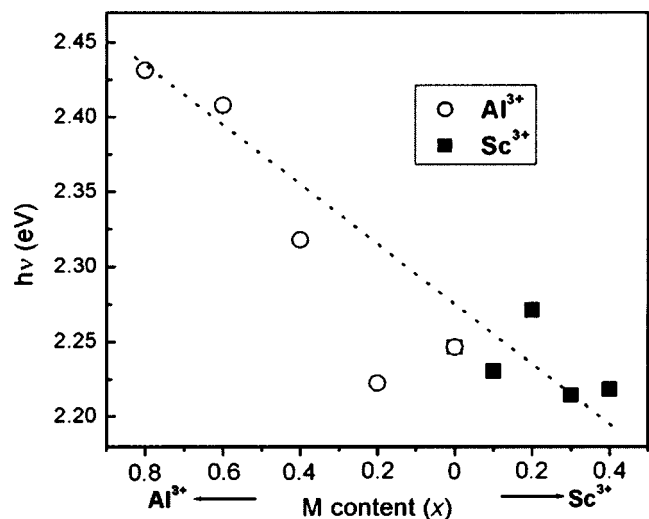


FIG. 11. Dependence of the energy of the IVCT transition ($[\text{Co}^{2+}] \rightarrow [\text{Fe}^{3+}]$) upon the doping content x for $\text{CoFe}_{2-x}\text{Al}_x\text{O}_4$ ($x = 0-0.8$) and $\text{CoFe}_{2-x}\text{Sc}_x\text{O}_4$ ($x = 0-0.4$) films annealed at 700°C for 1 h.

rotation peak attributed to the IVCT transition of $[\text{Co}^{2+}]t_{2g} \rightarrow \text{O}^{2-} \rightarrow [\text{Fe}^{3+}]t_{2g}$. Figure 11 shows the dependence of the energy of the IVCT transition upon the doping content x for $\text{CoFe}_{2-x}\text{Al}_x\text{O}_4$ ($x=0-0.8$) and $\text{CoFe}_{2-x}\text{Sc}_x\text{O}_4$ ($x=0-0.4$) films. It is obvious that the energy of the IVCT transition increased with x in $\text{CoFe}_{2-x}\text{Al}_x\text{O}_4$ films. The exception at $x=0.2$ is related to the perturbation of the spinel structure.^{5,6} However, the energy of the IVCT transition decreased with increasing x in $\text{CoFe}_{2-x}\text{Sc}_x\text{O}_4$ films. Therefore, we could conclude that doping with relatively small ions such as Al^{3+} ions would result in increasing the energy of the IVCT transition of $[\text{Co}^{2+}]t_{2g} \rightarrow \text{O}^{2-} \rightarrow [\text{Fe}^{3+}]t_{2g}$ in CoFe_2O_4 , and doping with relatively large ions such as Sc^{3+} ion would result in decreasing the energy of the IVCT transition.

By considering the results of the Rietveld refinement, the molecular orbital theory of IVCT transitions was introduced to interpret the above correlation between structures and $d-d$ IVCT transitions. According to this theory,^{14,15} 10 $3d$ orbitals of Co^{2+} and Fe^{3+} at B sites form 10 molecular orbitals, which are t_{2g} ($16a_1$, $10b_1$, $6a_2$, $7a_2$, $11b_1$, $17a_1$) and e_g ($18a_1$, $12b_2$, $19a_1$, $13b_2$) in a sequence showing increasing energy. The 12 $3d$ electrons (7 from Co^{2+} and 5 from Fe^{3+}) occupy 10 α spin and 2 β spin ($16a_1$ and $10b_1$) orbitals in the high-spin crystal field. Since the energy of the $3d$ orbital of Fe^{3+} ion is higher than that of Co^{2+} ion, the bonding orbitals of $16a_1$, $10b_1$ and $6a_2$ are mainly composed of $(3d)t_{2g}$ of Co^{2+} , and the antibonding orbitals of $7a_2$, $11b_1$ and $17a_1$ are mainly composed of $(3d)t_{2g}$ of Fe^{3+} . The Kerr rotation peak at 2.25 eV is the electronic transition from the molecular orbital $16a_1$ (σ bonding) to $17a_1$ (σ antibonding), which is the so-called IVCT transition of $[\text{Co}^{2+}]t_{2g} \rightarrow \text{O}^{2-} \rightarrow [\text{Fe}^{3+}]t_{2g}$. The energy gap between $16a_1$ and $17a_1$ is also the energy of the IVCT transition.

It is well known that the energy gap between bonding and antibonding is closely related to the distance between the bonding atoms.³⁹ Decreasing the distance between bonding atoms will decrease the energy of the bonding orbital and increase the energy of the antibonding orbital and thus increase the energy of electron transition from the bonding to antibonding orbital. On the other hand, increasing the distance between bonding atoms will decrease the energy gap, and the energy of bonding and antibonding orbital will be equal when the distance between two bonding atoms is infinite. Thinking about the IVCT transition of $[\text{Co}^{2+}]t_{2g} \rightarrow \text{O}^{2-} \rightarrow [\text{Fe}^{3+}]t_{2g}$ in CoFe_2O_4 and $\text{CoFe}_{2-x}M_x\text{O}_4$ ($M = \text{Mn, Al, Sc}$) thin films, the distance between Co^{2+} and Fe^{3+} ions (see the typical d_{B-B} values in Table I) will be decreased when doping with a relatively small ion such as the Al^{3+} ion, as is also confirmed by the Rietveld refinement. Therefore, the energy of the IVCT transition from $16a_1$ to $17a_1$ will be increased. On the other hand, the energy of the IVCT transi-

tion would be reduced when doped with relatively large ions such as Sc^{3+} ions due to the increased distance between Co^{2+} and Fe^{3+} ions at B sites. To sum up, doping with various trivalent metal ions can strongly affect the energy of the IVCT transition due to doping-induced structural changes, and hence adjust the position of Kerr rotation peak of CoFe_2O_4 .

V. CONCLUSION

By a modified Pechinii-type sol-gel method, we have fabricated nanocrystalline $\text{CoFe}_{2-x}M_x\text{O}_4$ ($M = \text{Mn, Al, Sc}$) thin films with well-crystallized spinel structure, and systematically investigated the correlation between structures and IVCT transitions. Structural studies revealed that doping of Mn^{3+} ions had a weak effect on both of the lattice and the nanocrystalline crystallization. However, doping of Al^{3+} ions resulted in a decrease in the lattice constant a , while the doping of Sc^{3+} ions brought about the increase in a . The doping of either Al^{3+} or Sc^{3+} ions could suppress the crystallization. Since Co^{2+} ions migrated from B to A sites due to the substitution of Fe^{3+} with M^{3+} , M_S and H_C of all the samples decreased with increasing doping content x .

MO investigations strongly suggested that doping with various trivalent metal ions could heavily affect the position of the Kerr rotation peak attributed to the IVCT transition of $[\text{Co}^{2+}]t_{2g} \rightarrow \text{O}^{2-} \rightarrow [\text{Fe}^{3+}]t_{2g}$ in CoFe_2O_4 thin films, within the miscibility range of spinel structure. The origin of the energy variations with the dopants can be understood by the molecular orbital theory of IVCT transitions. Since doping with the relatively small ions such as Al^{3+} could decrease the distance between Co^{2+} and Fe^{3+} ions, the energy gap (also the energy of the IVCT transition) between the molecular orbital $16a_1$ (σ) and $17a_1$ (σ^*) associated with the electron transition was increased. On the other hand, doping with the relatively large ions such as Sc^{3+} could increase the distance between Co^{2+} and Fe^{3+} ions, and decrease the energy gap. By understanding the above correlation between structures and IVCT transitions in the nanocrystalline $\text{CoFe}_{2-x}M_x\text{O}_4$ ($M = \text{Mn, Al, Sc}$) thin films, we conclude that the position of the Kerr rotation peak can be adjusted by doping various trivalent cations and controlling the doping content x due to doping-induced structural changes.

ACKNOWLEDGMENTS

Grants-in-aid from the State Key Project on Fundamental Research of MOST of China (G1998061300), NSFC (Nos. 50272006, 20171003, 20221101, and 20023005), the Training Project for Doctoral Students of MOE, and the Founder Foundation of Peking University are gratefully acknowledged.

*Author to whom correspondence should be addressed. Email address: chyan@chem.pku.edu.cn

¹J. Smit and H. P. J. Wijn, *Ferrites* (Philips Technical Library, Eindhoven, 1959).

²V. A. M. Brabers, in *Handbook of Magnetic Materials*, edited by K. H. J. Buschow (Elsevier Science, Amsterdam, 1995), Vol. 8, p. 199.

³X. X. Zhang, J. Schoenes, W. Reim, and P. Wachter, *J. Phys. C*

- 16**, 6055 (1983).
- ⁴H. Feil, *Solid State Commun.* **69**, 245 (1989).
- ⁵W. F. J. Fontijn, P. J. van der Zaag, M. A. C. Devillers, V. A. M. Brabers, and R. Metselaar, *Phys. Rev. B* **56**, 5432 (1997).
- ⁶W. F. J. Fontijn, P. J. van der Zaag, N. F. Feiner, R. Metselaar, and M. A. C. Devillers, *J. Appl. Phys.* **85**, 5100 (1999).
- ⁷W. F. J. Fontijn, P. J. van der Zaag, and R. Metselaar, *J. Appl. Phys.* **83**, 6765 (1998).
- ⁸P. J. van der Zaag, W. F. J. Fontijn, P. Gaspard, R. M. Wolf, V. A. M. Brabers, R. J. M. van der Veerdonk, and P. A. A. van der Heijden, *J. Appl. Phys.* **79**, 5936 (1996).
- ⁹M. Abe and M. Gomi, *J. Appl. Phys.* **53**, 8172 (1982).
- ¹⁰R. Ahrenkiel and T. Coburn, *IEEE Trans. Magn.* **MAG-11**, 1103 (1975).
- ¹¹N. Hiratsuka and M. Sugimoto, *IEEE Trans. Magn.* **MAG-23**, 3326 (1987).
- ¹²G. C. Allen and N. S. Hush, in *Progress in Inorganic Chemistry*, edited by F. A. Cotton (Interscience, New York, 1967).
- ¹³V. N. Antonov, B. N. Harmon, V. P. Antropov, A. Ya. Perlov, and A. N. Yaresko, *Phys. Rev. B* **64**, 134410 (2001).
- ¹⁴D. M. Sherman, *Phys. Chem. Miner.* **14**, 355 (1987).
- ¹⁵D. M. Sherman, *Phys. Chem. Miner.* **12**, 161 (1985).
- ¹⁶L. Stichauer, G. Gavaille, and Z. Simsa, *J. Appl. Phys.* **79**, 3645 (1996).
- ¹⁷K. Suzuki, T. Namikawa, and Y. Yamazaki, *Jpn. J. Appl. Phys., Part 1* **27**, 361 (1988).
- ¹⁸J. W. D. Martens, W. L. Peeters, H. M. van Noort, and M. Erman, *J. Phys. Chem. Solids* **46**, 411 (1985).
- ¹⁹J. W. D. Martens, W. L. Peeters, P. Q. J. Nederpel, and M. Erman, *J. Appl. Phys.* **55**, 1100 (1984).
- ²⁰W. L. Peeters and J. W. D. Martens, *J. Appl. Phys.* **53**, 8178 (1982).
- ²¹J. W. D. Martens and A. B. Voermans, *IEEE Trans. Magn.* **MAG-20**, 1007 (1984).
- ²²K. J. Kim, H. S. Lee, M. H. Lee, and S. H. Lee, *J. Appl. Phys.* **91**, 9974 (2002).
- ²³J. A. Dean, *Lange's Handbook of Chemistry*, 15th ed. (McGraw-Hill, New York, 1999).
- ²⁴B. Zhou, Y. W. Zhang, F. X. Cheng, C. S. Liao, C. H. Yan, L. Y. Chen, and S. Y. Wang, *Appl. Phys. Lett.* **79**, 1849 (2001).
- ²⁵B. Zhou, Y. W. Zhang, C. S. Liao, and C. H. Yan, *J. Magn. Magn. Mater.* **247**, 70 (2002).
- ²⁶F. X. Cheng, J. T. Jia, Z. G. Xu, B. Zhou, C. S. Liao, C. H. Yan, L. Y. Chen, and H. B. Zhao, *J. Appl. Phys.* **86**, 2727 (1999).
- ²⁷F. X. Cheng, J. T. Jia, C. S. Liao, Z. G. Xu, B. Zhou, C. H. Yan, L. Y. Chen, and H. B. Zhao, *J. Appl. Phys.* **87**, 6779 (2000).
- ²⁸M. Kakihana and M. Yoshimura, *Bull. Chem. Soc. Jpn.* **72**, 1427 (1999).
- ²⁹J. I. Langford, *J. Appl. Crystallogr.* **4**, 259 (1971).
- ³⁰J. I. Langford, *J. Appl. Crystallogr.* **6**, 190 (1973).
- ³¹A. Guinier, in *Theorie et Technique de la Radiocristallographie*, 3rd ed. (Dunod, Paris, 1964), p. 482.
- ³²G. A. Sawatzky, F. van der Woude, and A. H. Morrish, *Phys. Rev.* **187**, 747 (1969).
- ³³P. J. van der Zaag, A. Noordermeer, M. T. Johnson, and P. F. Bongen, *Phys. Rev. Lett.* **68**, 3112 (1992).
- ³⁴V. A. M. Brabers, *Phys. Rev. Lett.* **68**, 3113 (1992).
- ³⁵L. Bouet, P. Tailhades, and A. Rousset, *J. Magn. Magn. Mater.* **153**, 389 (1996).
- ³⁶K. M. Jadhav, V. B. Kawade, K. B. Modi, G. K. Bichile, and R. G. Kulkarni, *Physica B* **291**, 379 (2000).
- ³⁷J. W. D. Martens and W. L. Peeters, *Proc. SPIE* **420**, 231 (1983).
- ³⁸A. C. Larson and R. B. von Dreele, Los Alamos National Laboratory Report No. LAUR 86-748, 1986 (unpublished).
- ³⁹I. N. Levine, *Molecular Spectroscopy* (Wiley, New York, 1975).